Magnetic-field tailoring of the terahertz polarization emitted from a spintronic source

M. T. Hibberd,[1,2,a)] D. S. Lake,[1,2] N. A. B. Johansson,[3] T. Thomson,[3] S. P. Jamison,[2,4,5] and D. M. Graham[1,2]

[1)] *School of Physics and Astronomy & Photon Science Institute, The University of Manchester, Oxford Road, Manchester M13 9PL, UK*

[2)] *The Cockcroft Institute, Sci-Tech Daresbury, Keckwick Lane, Daresbury, Warrington WA4 4AD, UK*

[3)] *School of Computer Science, The University of Manchester, Oxford Road, Manchester M13 9PL, UK*

[4)] *Accelerator Science and Technology Centre, Science and Technology Facilities Council, Sci-Tech Daresbury, Keckwick Lane, Daresbury, Warrington WA4 4AD, UK*

[5)] *Department of Physics, Lancaster University, Bailrigg, Lancaster LA1 4YW, UK*

(Dated: 25 December 2018)

We demonstrate a method to create arbitrary terahertz (THz) polarization profiles by exploiting the magnetic field dependent emission process of a spintronic source. As a proof-of-concept, we show that by applying a specific magnetic field pattern to the source that it is possible to generate a quadrupole-like THz polarization profile. Experimental measurements of the electric field at the focus of the THz beam revealed a polarity flip in the transverse profile of the quadrupole-like mode with a resulting strong, on-axis longitudinal component of 17.7 kVcm^{-1}. This represents an order of magnitude increase in the longitudinal component for the quadrupole-like profile compared to a linear polarization, showing an example of how magnetic field patterning of a spintronic source can be exploited to obtain desirable THz polarization properties. This unique ability to generate any desired THz polarization profile opens up possibilities for schemes such as rotatable polarization spectroscopy and for efficient mode coupling in various waveguide designs. Furthermore, the strong longitudinal fields that can be generated have applications in areas including intra-subband spectroscopy of semiconductors, non-diffraction limited THz imaging and particle-beam acceleration.

The recent emergence of spintronic terahertz (THz) emitters has provided a low-cost source of high field-strength, broadband THz radiation.[1–5] As reported by Seifert *et al.*,[1] the emitters exploit laser-induced electron spin properties in magnetic multi-layers (see Fig. 1(a)) to produce gap-free emission covering 1-30 THz, with electric field amplitudes exceeding that generated in commonly-used non-linear crystals. In a further study,[5] amplified laser pulses were used to excite a large-area (7.5 cm diameter) spintronic source to produce electric fields of 0.3 MVcm^{-1} measured at the focus of the THz beam. Under similar excitation and focussing conditions, field strengths of 1.2 MVcm^{-1} have been reported using a tilted-pulse-front-pumping (TPFP) scheme in lithium niobate (LN) crystals.[6] Given the relative cost and the complexity involved in TPFP of a LN source, together with the potential for significant development of only-recently established spintronic emitters, the comparative THz electric field values on the order of MVcm^{-1} are extremely promising for future high-field applications operating in the THz-induced non-linear regime[7–9].

A unique property of spintronic emitters is that they have been shown to generate THz radiation polarized perpendicular to the moment of the magnetic structure but independent of the pump laser polarization.[1,2] In order to manipulate the magnetic moment, a magnetic field is applied to the source and fields on the order of 10 mT are sufficient to saturate the magnetic structure. To date, sources have been placed between two permanent magnets of aligned polarity, producing linearly polarized THz radiation as a result of the magnetic moment aligning to the straight magnetic field lines running parallel to the source plane. However, this polarization dependence on the magnetic state of the source offers the potential to directly tailor an arbitrary polarization profile of the emitted THz radiation by controlling the applied magnetic field pattern.

The arbitrary control of THz polarization, and the ability to generate unique polarization profiles, have numerous potential applications in THz spectroscopy and coherent control over material structure and dynamics,[9,10] with examples including THz-assisted asymmetric synthesis of chiral molecules[11], THz-driven electron-hole re-collisions[12], ferroelectric domain switching[13], ultrafast manipulation of collective spin excitations[14] and rotatable polarization spectroscopy[15]. Additionally, more complex modes with radial polarization offer high-efficiency coupling of THz radiation to cylindrical wire waveguides[16], and when focussed also provide enhanced longitudinal electric field components[17]. While basic THz polarization control can be achieved using optical components such as wire-grid polarizers[18] and waveplates[19], more complex control has recently been demonstrated by Sato *et al.*[20]. A spatial light modulator (SLM) was used to modify a near-infrared laser pulse and subsequently imprint a prescribed polarization state onto the THz field generated from a non-linear crystal.[20] However, despite the variety of achievable polarization-shaped waveforms, the scheme relied on complex optical components, with the SLM-based setup restricting the bandwidth, pulse duration

[a)] Electronic mail: morgan.hibberd@manchester.ac.uk

and peak intensity of the generated THz waveforms. This resulted in a maximum THz field amplitude limited to 300 Vcm^{-1}.

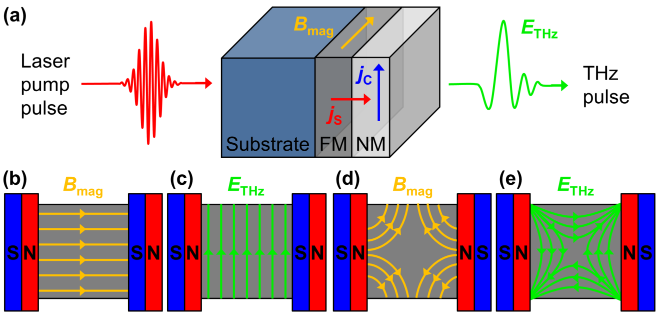

FIG. 1. (a) Mechanism of THz generation from a spintronic source. A laser pump pulse launches a spin-polarized current (j_S) in the ferromagnetic (FM) layer that is converted to a transverse charge current (j_C) in the non-ferromagnetic (NM) layer, generating a THz pulse polarized perpendicular to the applied magnetic field (B_{mag}). (b)-(e) Schematic diagrams of the two permanent magnets on either edge of a spintronic source, showing the magnetic field lines when oriented with (b) aligned and (c) opposing polarity. The corresponding THz electric field lines are given in (d) and (e), respectively.

In this letter, we demonstrate the ability to generate high-field strength THz radiation with arbitrary polarization profiles, and without the use of complex optical components. We report on the application of a magnetic field pattern to a spintronic emitter placed between two magnets of either aligned or opposing polarity, which after excitation of the emitter by a femtosecond laser pulse, results in the generation of THz radiation with either linear or quadrupole-like polarization, respectively. Our findings demonstrate that the THz polarization emitted from a spintronic source can be directly tailored by an applied magnetic field pattern to create a range of THz polarization profiles.

The spintronic source used in the experiment was a square 25x25 mm metallic bilayer structure consisting of a 2 nm-thick $Ni_{80}Fe_{20}$ FM bottom layer with a 2 nm-thick Pt NM top layer, deposited on a 500 μm-thick MgO substrate by DC-magnetron sputtering. The FM layer was chosen due to the low coercivity of $Ni_{80}Fe_{20}$ (see supplementary material), enhancing the ability to manipulate the magnetic structure of the layer with weak magnetic fields compared to materials of higher coercivity. Furthermore, measurements with varying $Ni_{80}Fe_{20}$ layer thickness from 1-5 nm showed the 2 nm layer gave the highest THz electric field amplitude (see supplementary material), in agreement with Seifert *et al.*[1], who reported a peak in the THz amplitude for a total bilayer thickness of 4 nm. The applied magnetic field was provided by two 25 mm-diameter, 2 mm-thick neodymium (N42) disc magnets, with the north and south pole on each magnet located on each circular face. As shown in Fig. 1(b)-(e), the two magnets were placed on either edge of the spintronic source and were separated by approximately 25 mm. In the case of Fig. 1(b) for aligned magnetic polarity (opposite poles oriented towards the source such that the magnets attract each other), a magnetic field in the centre of approximately 50 mT decreasing to 20 mT at the edges was measured using a Hall probe. The applied magnetic field was therefore always in excess of the saturating field of the ferromagnetic $Ni_{80}Fe_{20}$ layer, measured using the magneto-optic Kerr effect to be approximately 5 mT (see supplementary material). To achieve opposing magnetic polarity, the orientation of one magnet was reversed and the resulting magnetic field pattern is illustrated in Fig. 1(d). For the experiment, the spintronic source was mounted on a perspex plate with a 23 mm clear aperture and all measurements were taken unpurged at room temperature with the pump beam incident from the substrate side.

The experimental setup employed a 1 kHz regenerative amplifier system, which produced 6.5 mJ of 800 nm radiation with a pulse duration of 45 fs. The laser beam was split into a pump (90%) and probe (10%) for THz generation and detection, respectively. A schematic diagram of the experimental setup is shown in Fig. 2, with a collimated 10 mm diameter, 1.3 mJ pump beam (pump fluence = 1.65 mJcm^{-2}) used to excite the spintronic source. An indium-tin-oxide (ITO)-coated glass plate was used to reflect the emitted THz radiation, whilst transmitting the majority of the remaining 800 nm pump beam towards a beam block. A high-resistivity float-zone silicon (Si) wafer was used to remove any residual 800 nm pump radiation. The THz radiation was then focussed by a 25 mm-diameter gold

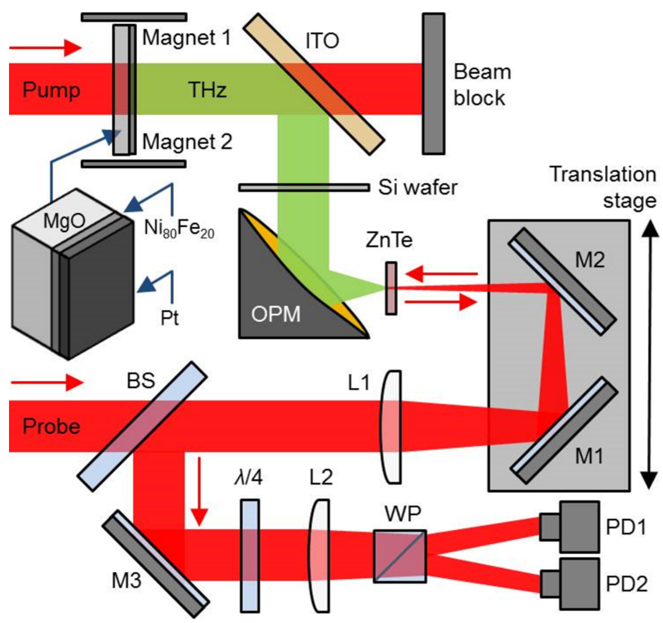

FIG. 2. Schematic diagram of the experimental setup showing the pump and probe beam paths used for THz generation and detection, respectively. Details are given in the main text. M = mirror, L = lens, BS = beamsplitter, $\lambda/4$ = quarter-waveplate, WP = Wollaston prism, PD = photodiode.

90° off-axis parabolic mirror (OPM) with focal length of 25 mm onto a 500 μm-thick ZnTe electro-optic crystal. For THz detection, the probe beam was focussed (L1 focal length = 1000 mm) onto the ZnTe crystal in a back-reflection geometry. An 800 nm anti-reflection coating on the back face of the ZnTe crystal allowed the probe beam to transmit and subsequently reflect back off the front face of the crystal to co-propagate with the incident THz radiation. A 50:50 beamsplitter was used to direct the back-reflected probe beam into a standard electro-optic detection scheme. To enable spatial profiling of the THz beam on the ZnTe crystal, mirrors M1 and M2 were positioned on a computer-controlled translation stage, which provided horizontal translation of the probe beam without altering the path length.

The results in Fig. 3 show the transverse THz electric field waveforms and corresponding spectral amplitudes measured at the focus of the THz beam, as a function of horizontal sampling position across a (110)-cut ZnTe detection crystal. The THz electric field values were calculated from the THz-induced intensity change recorded on the photodiodes[21] and accounted for the measured 67% THz amplitude transmission of the Si wafer, used to block the residual pump radiation. In Fig. 3(a) and (b)

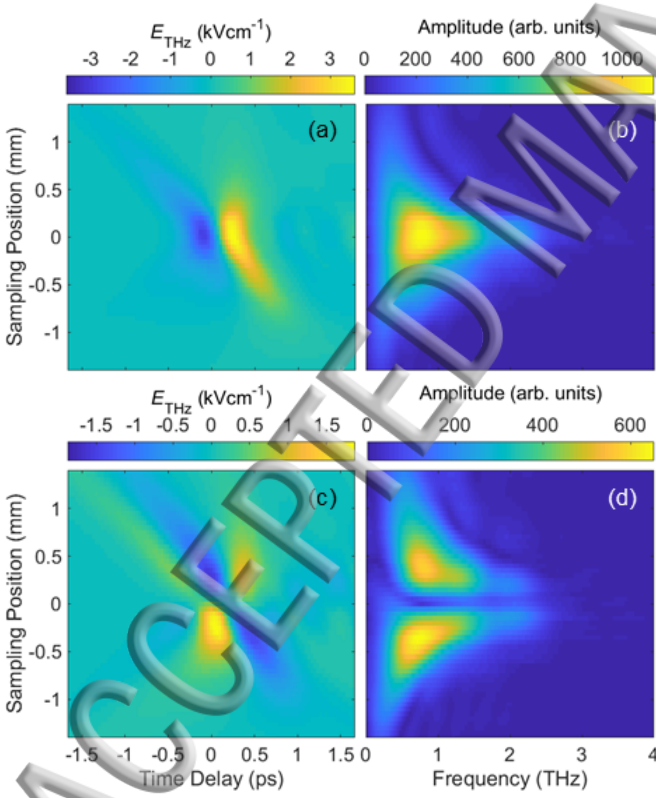

FIG. 3. Transverse THz waveforms measured at the THz beam focus, as a function of horizontal sampling position on a ZnTe (110)-cut detection crystal for the spintronic source placed between magnets with (a) aligned and (c) opposing polarity. The corresponding spectral amplitudes are given in (b) and (d), respectively.

the spintronic source was placed between two magnets with aligned polarity, which as illustrated in Fig. 1(b), produced horizontal magnetic field lines running parallel to the source plane. The magnetic domains in the ferromagnetic $Ni_{80}Fe_{20}$ layer aligned to the direction of these magnetic field lines and, after excitation of the source with a laser pump pulse, resulted in the generation of vertically polarized THz radiation, as shown by Fig. 1(c). The azimuthal angle of the ZnTe (110)-cut crystal was therefore set to maximize detection for this polarization. As seen in Fig. 3(a) and (b), the transverse components of the vertically polarized THz radiation focus to a spot with FWHM of 0.65 mm at 1 THz, a peak on-axis E_{THz} value of 3.6 kVcm^{-1} and spectral bandwidth extending up to approximately 2.5 THz, limited by the 500 μm-thick ZnTe detection crystal. In Fig. 3(c) and (d), one of the magnets was reversed to create an opposing magnetic polarity configuration, which resulted in a magnetic field pattern in the source plane given by Fig. 1(d). Due to the low coercivity of the $Ni_{80}Fe_{20}$ layer (see supplementary material), to good approximation the magnetic domains align with the direction of the magnetic field lines, producing the THz electric field pattern shown in Fig. 1(e). The impact of this quadrupole-like THz polarization profile on the focussed THz beam can be seen in Fig. 3(c) and (d), where a polarity flip in E_{THz} along the horizontal sampling axis results in a zero on-axis transverse THz electric field and approximately equal splitting into positive and negative lobes with peak E_{THz} values of 1.9 kVcm^{-1} and -1.6 kVcm^{-1}, respectively. The THz focal field distribution and magnitude were not sensitive to small variations in magnet alignment and were easily repeated with the magnets removed and reinstalled between measurements.

Further measurements were performed using a (100)-cut ZnTe detection crystal to investigate the longitudinal components of the THz electric field, where the calculation of E_{THz} required the Fresnel amplitude transmission coefficient for longitudinally polarized THz radiation,[22] given by $t_{\mathrm{long}} = 2/n_{\mathrm{THz}}(1 + n_{\mathrm{THz}})$, with the results shown in Fig. 4. In the case of aligned magnetic polarity in Fig. 4(a), the longitudinal components are almost an order of magnitude weaker than the transverse components observed in Fig. 3(a), with the maximum longitudinal E_{THz} amplitude only reaching a value of 0.54 kVcm^{-1}. Such weak longitudinal components are expected for linearly polarized THz radiation, arising from transverse gradients in the beam profile[23]. The slight asymmetry in the spatial profile is attributed to a small misalignment in the THz beam focusing but the expected polarity flip with zero on-axis longitudinal THz electric field can be distinguished from the spectral components in Fig. 4(b). In contrast, for an opposing magnetic polarity configuration in Fig. 4(c) and (d), the longitudinal components of the quadrupole-like THz radiation focus to a spot with FWHM of 0.68 mm at 1 THz and a peak on-axis E_{THz} value of 7.0 kVcm^{-1}. This peak longitudinal value for the quadrupole-like THz polariza-

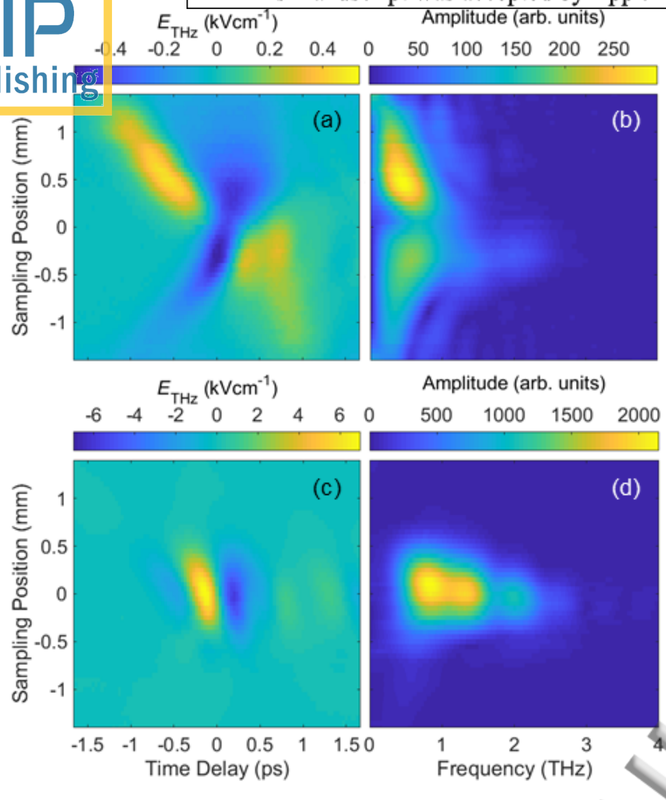

FIG. 4. Longitudinal THz waveforms measured at the THz beam focus, as a function of horizontal sampling position on a ZnTe (100)-cut detection crystal for the spintronic source placed between magnets with (a) aligned and (c) opposing polarity. The corresponding spectral amplitudes are given in (b) and (d), respectively.

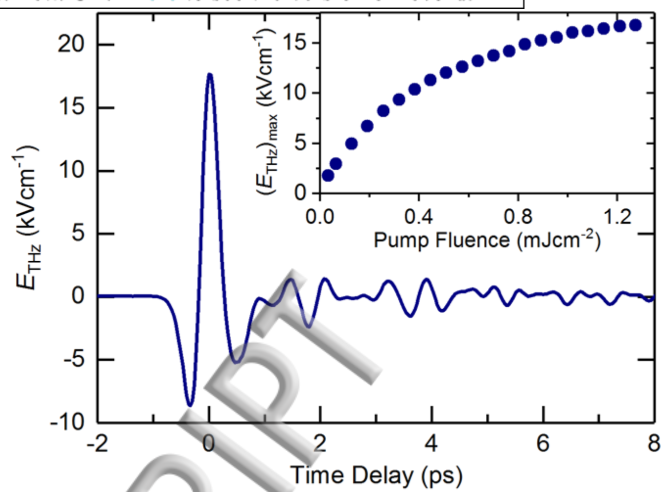

FIG. 5. Peak longitudinal THz waveform measured with a ZnTe (100) detection crystal. Inset: Dependence of the peak THz electric field amplitude on the pump fluence.

tion mode not only exceeds its transverse counterpart in Fig. 3(c) but is almost double the peak 3.6 kVcm^{-1} transverse E_{THz} for vertically polarized THz radiation in Fig. 3(a). Therefore, these results demonstrate that over an order of magnitude increase in the peak longitudinal E_{THz} can be achieved at the focus of the THz beam if a suitable magnetic field pattern is utilized with a spintronic emitter. The expected $\pi/2$ phase shift between the transverse and longitudinal components[23] observed in Fig. 3(c) and Fig. 4(c), confirm that the longitudinal THz electric field components were measured.

Currently, there is significant interest in the use of intense THz radiation for particle acceleration[24–26] with the requirement of a strong longitudinal THz electric field component. As demonstrated from Fig. 4(c), such a component can be generated using a spintronic emitter placed between two magnets of opposing polarity. To maximize this peak E_{THz} value, the experimental setup was modified using a telescope to increase the diameter of the pump beam by a factor of 2 up to a FWHM of 20 mm. Consequently, a 4 mJ pump beam could be used for excitation without exceeding the pump fluence damage threshold of the spintronic emitter, estimated to be approximately 2 mJcm^{-2}. From the resulting transverse THz beam profile and field strength, the THz pulse energy was estimated to be on the order of 1 nJ, with the on-axis, longitudinal THz electric field waveform shown in Fig. 5, giving a peak value for E_{THz} of 17.7 kVcm^{-1}. This value exceeds that reported in previous work where schemes using THz air-plasma generation[27], a large-area photoconductive radial antenna[22] and the interferometric combination of two linearly polarized THz beams generated from a matched pair of LN crystals[28] were employed. Those schemes exploit large transverse field gradients, arising from a polarity flip in the transverse polarization, to produce intense longitudinal fields at the focus of the THz beam. While we observe a similar polarity flip in the transverse fields, from the symmetry of our quadrupolar THz emission profile, longitudinal fields are not expected to be directly generated from the transient divergence of the THz electric field, but rather are attributed to the transient charge build-up from current gradients.

In summary, we have demonstrated a proof-of-principle concept that a magnetic field pattern can be applied to a spintronic source to manipulate the magnetic state of the ferromagnetic layer, such that when the source is excited with a laser pulse, the transverse polarization profile of the resulting emitted THz radiation can be directly tailored. We have shown that when the source is placed between two magnets of opposing polarity, THz radiation with a quadrupole-like polarization profile can be generated, which when focussed results in longitudinal THz electric field amplitudes double that of the transverse THz electric fields achieved with linearly polarized THz radiation. Together with recent reports of transverse fields of 0.3 MVcm^{-1} from an optimized trilayer spintronic source[5], our results suggest that longitudinal fields approaching the order of 1 MVcm^{-1} are possible, making magnetic-field tailored spintronic sources a candidate for applications requiring an intense longitudinal THz field component. As a future outlook, while our proof-of-principle demonstration utilized a specific magnetic field pattern, it is possible to create any desired THz polarization profile by exploiting alternative magnetic field patterns applied to the spintronic source. This unique ability opens up numerous possibilities in areas including spectroscopy, imaging and particle-beam manipulation in the THz spectral range.

See supplementary material for experimental measurements of the optimal ferromagnetic layer thickness of the spintronic bilayer structure, and subsequent characterization of the magnetic properties of the chosen structure.

This work was supported by the United Kingdom Science and Technology Facilities Council [Grant Nos. ST/N00308X/1 and ST/P002056/1]. The data associated with the paper are openly available from the Mendeley Data Repository at: http://dx.doi.org/xx.xxxxx/x.xxxxxx.

[1] T. Seifert, S. Jaiswal, U. Martens, J. Hannegan, L. Braun, P. Maldonado, F. Freimuth, A. Kronenberg, J. Henrizi, I. Radu, E. Beaurepaire, Y. Mokrousov, P. M. Oppeneer, M. Jourdan, G. Jakob, D. Turchinovich, L. M. Hayden, M. Wolf, M. Münzenberg, M. Kläui, and T. Kampfrath, Nat. Photonics **10**, 483 (2016).
[2] D. Yang, J. Liang, C. Zhou, L. Sun, R. Zheng, S. Luo, Y. Wu, and J. Qi, Adv. Optical Mater. **4**, 1944 (2016).
[3] Y. Wu, M. Elyasi, X. Qiu, M. Chen, Y. Liu, L. Ke, and H. Yang, Adv. Mater. **29**, 1603031 (2016).
[4] T. J. Huisman and T. Rasing, J. Phys. Soc. Jpn. **86**, 011009 (2017).
[5] T. Seifert, S. Jaiswal, M. Sajadi, G. Jakob, S. Winnerl, M. Wolf, M. Kläui, and T. Kampfrath, Appl. Phys. Lett. **110**, 252402 (2017).
[6] H. Hirori, A. Doi, F. Blanchard, and K. Tanaka, Appl. Phys. Lett. **98**, 091106 (2011).
[7] H. Y. Hwang, S. Fleischer, N. C. Brandt, B. G. Perkins-Jr., M. Liu, K. Fan, A. Sternbach, X. Zhang, R. D. Averitt, and K. A. Nelson, J. Mod. Opt. **62**, 1447 (2015).
[8] H. A. Hafez, X. Chai, A. Ibrahim, S. Mondal, D. Férachou, X. Ropagnol, and T. Ozaki, J. Opt. **18**, 093004 (2016).
[9] T. Kampfrath, K. Tanaka, and K. A. Nelson, Nat. Photonics **7**, 680 (2013).
[10] T. L. Cocker and R. Huber, Nat. Photonics **7**, 678 (2013).
[11] Y. Fujimura, L. González, K. Hoki, J. Manz, and Y. Ohtsuki, Chem. Phys. Lett. **306**, 1 (1999).
[12] B. Zaks, R. B. Liu, and M. S. Sherwin, Nature **483**, 580 (2012).
[13] T. Qi, Y.-H. Shin, K.-L. Yeh, K. A. Nelson, and A. M. Rappe, Phys. Rev. Lett. **102**, 247603 (2009).
[14] T. Kampfrath, A. Sell, G. Klatt, A. Pashkin, S. Mährlein, T. Dekorsy, M. Wolf, M. Fiebig, A. Leitenstorfer, and R. Huber, Nat. Photonics **5**, 31 (2011).
[15] C. D. W. Mosley, M. Failla, D. Prabhakaran, and J. Lloyd-Hughes, Sci. Rep. **7**, 12337 (2017).
[16] J. A. Deibel, K. Wang, M. D. Escarra, and D. M. Mittleman, Opt. Express **14**, 279 (2006).
[17] R. Imai, N. Kanda, T. Higuchi, Z. Zheng, K. Konishi, and M. Kuwata-Gonokami, Opt. Express **20**, 21896 (2012).
[18] N. Amer, W. C. Hurlbut, B. J. Norton, and Y.-S. Lee, Appl. Phys. Lett. **87**, 221111 (2005).
[19] J.-B. Masson and G. Gallot, Opt. Lett. **31**, 265 (2006).
[20] M. Sato, T. Higuchi, N. Kanda, K. Konishi, K. Yoshioka, T. Suzuki, K. Misawa, and M. Kuwata-Gonokami, Nat. Photonics **7**, 724 (2013).
[21] P. C. M. Planken, C. E. W. M. van Rijmenam, and R. N. Schouten, Semicond. Sci. Technol. **20**, S121 (2005).
[22] M. J. Cliffe, A. Rodak, D. M. Graham, and S. P. Jamison, Appl. Phys. Lett. **105**, 191112 (2014).
[23] S. Winnerl, R. Hubrich, M. Mittendorff, H. Schneider, and M. Helm, New J. Phys. **14**, 103049 (2012).
[24] E. A. Nanni, W. R. Huang, K.-H. Hong, K. Ravi1, A. Fallahi, G. Moriena, R. J. D. Miller, and F. X. Kärtner, Nat. Commun. **6**, 8486 (2015).
[25] C. Kealhofer, W. Schneider, D. Ehberger, A. Ryabov, F. Krausz, and P. Baum, Science **352**, 429 (2016).
[26] D. A. Walsh, D. S. Lake, E. W. Snedden, M. J. Cliffe, D. M. Graham, and S. P. Jamison, Nat. Commun. **8**, 421 (2017).
[27] Y. Minami, T. Kurihara, K. Yamaguchi, M. Nakajima, and T. Suemoto, Appl. Phys. Lett. **102**, 151106 (2013).
[28] M. J. Cliffe, D. M. Graham, and S. P. Jamison, Appl. Phys. Lett. **108**, 221102 (2016).


(a)
Laser pump pulse
B mag
j c
j s
Substrate
FM
NM
E THz
THz pulse
(b)
B mag
S N
S N
(c)
E THz
S N
S N
(d)
B mag
S N
N S
(e)
E THz
S N
N S

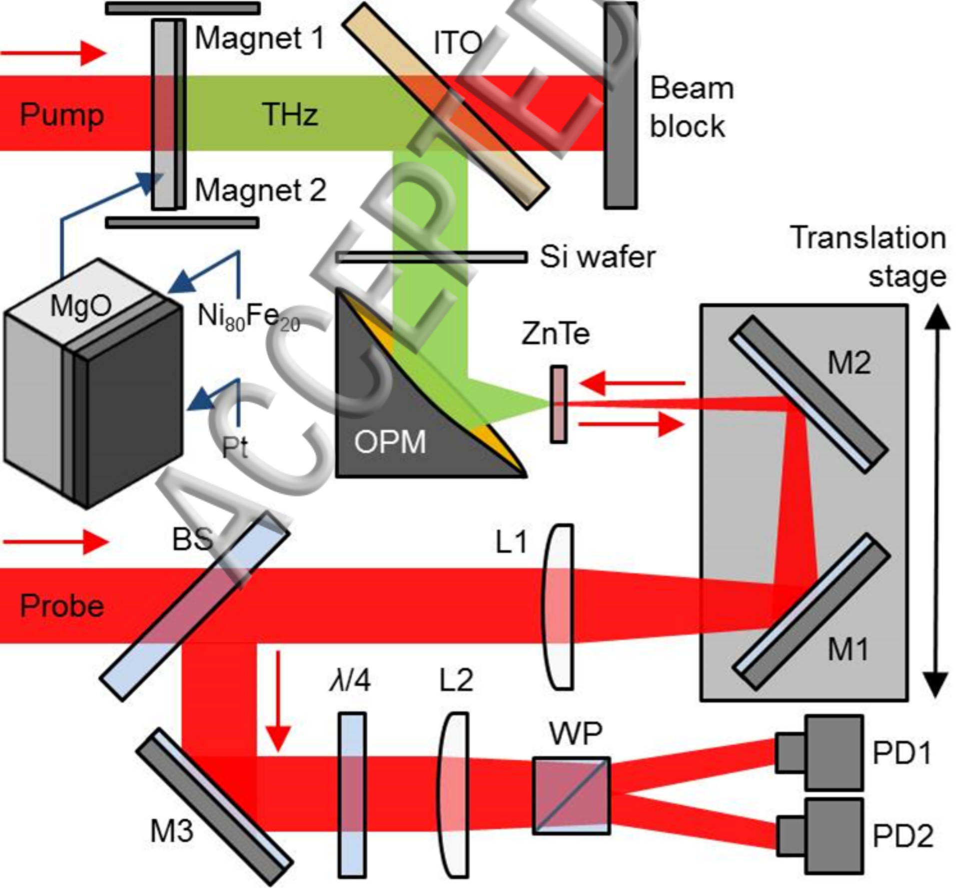
Magnet 1
ITO
Pump
THz
Beam
block
Magnet 2
Translation
stage
Si wafer
MgO
Ni80Fe20
ZnTe
M2
Pt
OPM
BS
L1
Probe
M1
λ/4
L2
WP
PD1
M3
PD2

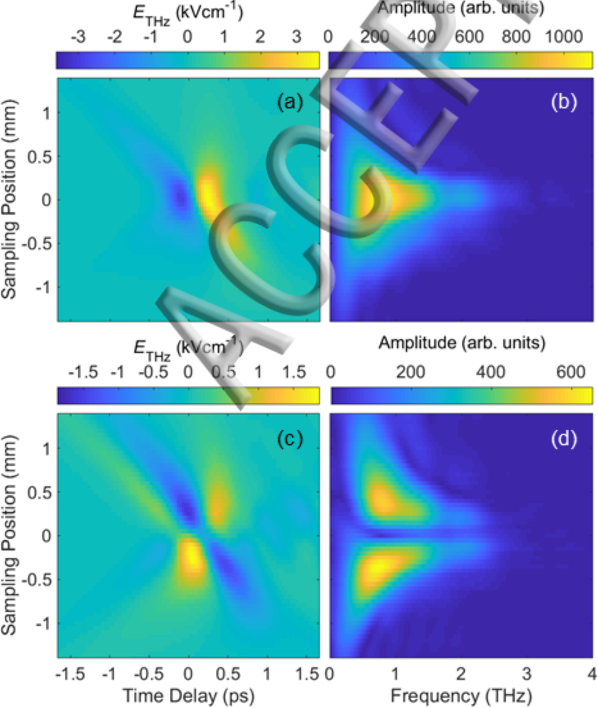

E_{THz} (kVcm^{-1})
-3 -2 -1 0 1 2 3
Amplitude (arb. units)
0 200 400 600 800 1000
(a)
(b)
Sampling Position (mm)
1 0.5 0 -0.5 -1
E_{THz} (kVcm^{-1})
-1.5 -1 -0.5 0 0.5 1 1.5
Amplitude (arb. units)
0 200 400 600
(c)
(d)
-1.5 -1 -0.5 0 0.5 1 1.5
Time Delay (ps)
0 1 2 3 4
Frequency (THz)
ACCEPTED

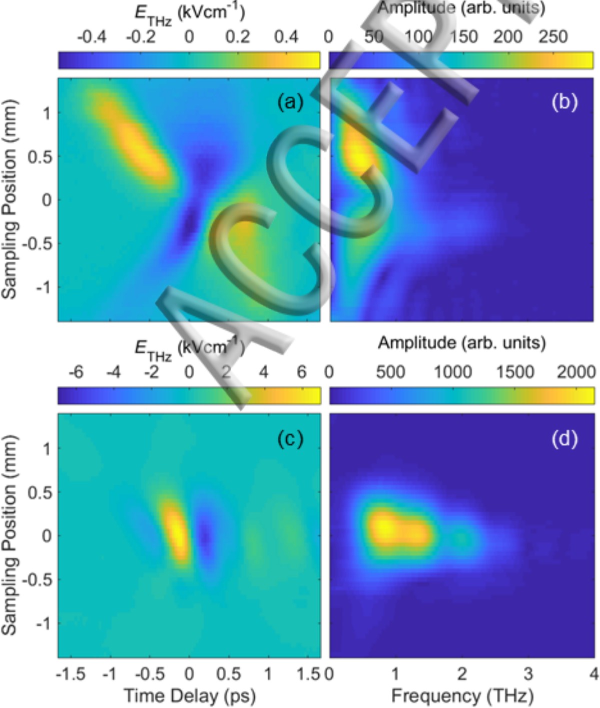

E_{THz} (kVcm^{-1})
-0.4 -0.2 0 0.2 0.4
Amplitude (arb. units)
0 50 100 150 200 250
(a)
(b)
Sampling Position (mm)
1 0.5 0 -0.5 -1
E_{THz} (kVcm^{-1})
-6 -4 -2 0 2 4 6
Amplitude (arb. units)
0 500 1000 1500 2000
(c)
(d)
Sampling Position (mm)
1 0.5 0 -0.5 -1
-1.5 -1 -0.5 0 0.5 1 1.5
Time Delay (ps)
0 1 2 3 4
Frequency (THz)

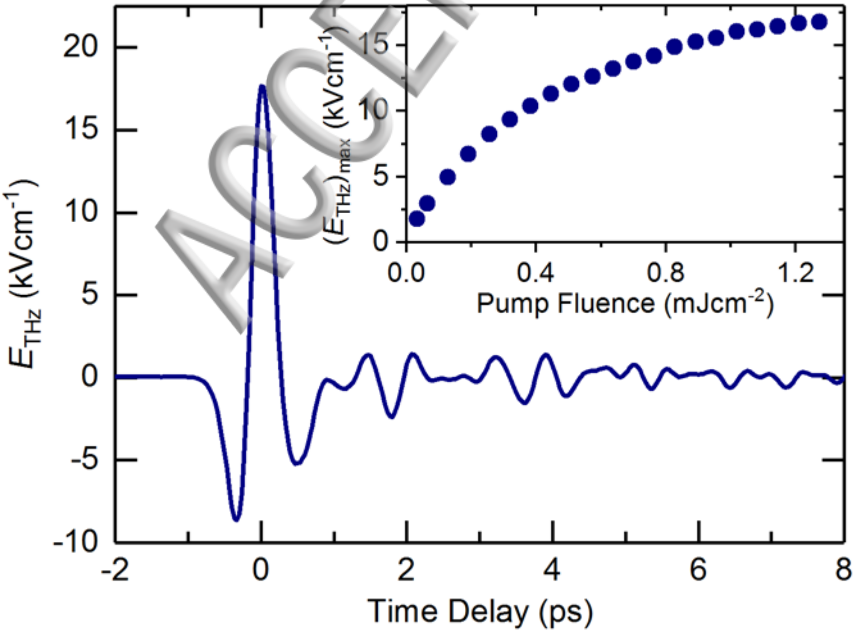

E_{THz} (kVcm^{-1})
Time Delay (ps)
$(E_{THz})_{max}$ (kVcm^{-1})
Pump Fluence (mJcm^{-2})
ACCEPTED